

Influence of Heat Treatments on the Microstructure and Mechanical Properties of Two Fine Mg–Li–Y Alloy Wires for Bioresorbable Applications

Kenneth MacLeod,* David H. Nash, David R. Bow,* and Le Ma

Two Mg–4Li– x Y ($x = 0.5$ and 2.0 wt%) alloy wires are investigated for application in bioresorbable medical devices that experience high levels of plastic deformation. The two wires are supplied cold drawn to a diameter of $125\ \mu\text{m}$, and a series of thermal treatments are applied to maximize ductility. The ductility of the alloys is maximized soon after complete recrystallization. Prolonged annealing causes grain coarsening in the Mg–4Li–0.5Y alloy and precipitation of a Mg_{24}Y_5 phase in both alloys. Both wires are shown to achieve $\approx 20\%$ elongation to failure in tension and survive high idealized bending strains ($>40\%$). When heat treated for optimum mechanical properties for the intended application, the Mg–4Li–0.5Y alloy develops an intense transverse basal texture; however, this is shown to weaken with increased Y content in the Mg–4Li–2Y alloy wire. The increased Y content also prevents grain coarsening, indicating that the increased Y content restricts grain boundary mobility during annealing. Both alloys have relatively high ductility, meaning both are identified as promising new materials for application in bioresorbable medical devices that require to achieve and support high levels of plastic deformation during their life cycle.

and manufacture of the final device.^[3] Currently, the most effective protocol for fabricating fine Mg wires is through cold drawing extruded rods.^[4,5] The severe cold work (CW) imparted during this process generates a fibrous grain structure, commonly with an uneven internal stress distribution through the cross section of the wire: internal stress increasing toward the outer diameter (OD).^[6,7] The dominance of basal slip in Mg alloy wires causes this fibrous microstructure to develop a basal texture, whereby the grains tend to align with their c -axis perpendicular to the drawing direction (DD), causing the wires to exhibit high strength, low ductility, and anisotropic properties.^[8–10] A post drawing heat treatment process is essential, to improve the mechanical properties for further processing during manufacture of the final device. Alloying

is required to improve the formability of pure Mg to first survive the cold drawing process and then provide the ductility necessary for application in medical devices that undergo high levels of plastic deformation, such as wire form bioresorbable vascular scaffolds.^[4,7,10,11]


The mechanical properties of Mg can be improved through various alloying additions including Al, Zn, Ca, Li, and rare earth (RE) elements depending on the final requirements and usage.^[12] RE elements have been shown to improve the mechanical properties of Mg alloys through precipitation and solid solution strengthening, as well as weakening of the strong basal texture.^[13] Y, Gd, Dy, and Nd are four of the most common RE elements considered for bioresorbable materials owing to their relative bio-safety and ability to improve the mechanical properties and corrosion behavior of Mg alloys.^[14,15] Precipitation strengthening is an effective method to increase the strength of Mg and is common in the design of MgRE alloys. Age hardening is generally applied to induce the formation of precipitates in Mg alloys and is commonly conducted at temperatures between 100 and $300\ ^\circ\text{C}$ in order to develop the preferred size, morphology, density, orientation, and structure of precipitates to obtain the desired hardening effect.^[16] As well as providing a strengthening effect, particles can also act, both to suppress and promote recrystallization. The Zener pinning effect describes the mechanism of how small particles act to restrict the mobility of grain and subgrain boundaries that can slow the recrystallization process. However, secondary phase particles

1. Introduction

Interest in magnesium (Mg) alloy wires for use in a range of bioabsorbable implants is growing, owing to their biocompatibility, suitable corrosion rates, and good mechanical properties.^[1,2] The hexagonal close packed (HCP) crystal structure of Mg limits the formability of pure Mg at room temperature that can be improved through altering alloying and processing routes applied during both the fabrication of the Mg alloy wires

K. MacLeod, D. H. Nash, D. R. Bow
Department of Mechanical and Aerospace Engineering
University of Strathclyde
Glasgow G1 1XJ, UK
E-mail: kenneth.macleod.2014@uni.strath.ac.uk;
david.r.bow@strath.ac.uk

L. Ma
Sorby Centre, Department of Materials Science and Engineering
University of Sheffield
Broad Lane, Sheffield S3 7HQ, UK

 The ORCID identification number(s) for the author(s) of this article can be found under <https://doi.org/10.1002/adem.202201164>.

© 2022 The Authors. Advanced Engineering Materials published by Wiley-VCH GmbH. This is an open access article under the terms of the Creative Commons Attribution License, which permits use, distribution and reproduction in any medium, provided the original work is properly cited.

DOI: 10.1002/adem.202201164

>1 μm in size can facilitate the build-up of high-density dislocations, acting as potential nucleation sites for new grains during thermal processing.^[17,18] Zhang et al.^[19] showed that an Mg–2Sm–0.8Mn–0.6Ca–0.5Zn alloy exhibits both high strength and ductility following appropriate processing, through both precipitation strengthening, and restricted grain growth. Uniformly distributed Mn particles within the Mg matrix caused strengthening. While grain growth was restricted through the segregation of Sm, Ca, and Zn to high-angle boundaries, causing a fine-grained microstructure to develop during recrystallization, resulting in high strength and ductility of the alloy.^[19] Concurrent recrystallization and precipitation have been observed by Guan et al.^[20] during static recrystallization of cold rolled WE43 at temperatures up to 490 °C. Precipitation was observed along prior grain and twin boundaries during annealing, and these precipitates coarsened with extended time at high temperatures, before dissolving in the matrix following prolonged annealing. The authors suggested that high residual strain and solute segregation along grain and twin boundaries were responsible for the concurrent precipitation and recrystallization. They suggest that the nucleation and growth of precipitates were promoted to relieve the high strain energy along prior boundaries enriched with RE elements.^[20] Y and Gd are two of the most effective elements for solid solution strengthening, owing to the strong bonds they form with the Mg atoms.^[21] Further, alloying with Y has been shown to improve the corrosion resistance of Mg alloys in vitro, when the Y is in solution, through forming a stable oxide layer on the surface during corrosion.^[22] However, as Y is precipitated out of solution, it activates localized galvanic corrosion that increases the corrosion rate.^[23] Localized galvanic corrosion should be avoided when considering developing alloys for bioresorbable applications as it can result in premature failure of the device.^[24,25] Following thermal processing of MgRE alloys, a more random texture can be recrystallized, termed the “RE texture,” which improves ductility and reduces the anisotropy of these alloys.^[26] The origin of the RE texture is not fully understood; however, it has been shown that its appearance post thermal treatment can depend upon the previous processing steps, composition of RE elements in the alloy, and the annealing temperature.^[27,28] Studies concerning fine MgRE alloy wires, however, have not shown that recrystallization of the RE texture is achievable in severely cold drawn wires, which is attributed to the high level of deformation imparted on the wires during drawing.^[7,8,10,29]

This study seeks to investigate the suitability of two Mg–Li–Y alloy wires, with varying Y content, for application in bioresorbable medical devices that undergo high levels of plastic deformation. Li and Y were selected as they are both shown to improve the mechanical properties of Mg and are considered safe in vivo within the alloying limits investigated in this study.^[15,30] Li improves the ductility of Mg alloys through increased activation of non-basal slip, caused by reducing the c/a axis ratio of the HCP unit cell, when alloyed below 5.5 wt%. Above this limit, a Li-rich beta phase forms that further improves ductility but reduces both strength and corrosion resistance.^[31,32] Y was selected to increase the strength of the alloy through solid solution strengthening, to avoid any galvanic corrosion or limited ductility that is associated with precipitation hardened alloys. Further, through alloying with Y, it is desired that some weakening of the strong basal

texture can be achieved. This study seeks to optimize a heat treatment process both Mg–Li–Y alloy wires to maximize their ductility. The effect these treatments have on the microstructure and mechanical properties of the two alloy wires is investigated, and conclusions are drawn on their suitability for application in medical devices that undergo severe plastic deformation.

2. Experimental Section

2.1. Materials

Two Mg–Li–Y alloy wires with compositions by weight of Mg–4Li–0.5Y (0.5Y) and Mg–4Li–2Y (2Y) were provided cold drawn to a diameter of 125 μm. The 0.5Y and 2Y wires were supplied with the final drawing step imparting 80 and 65% CW, respectively. A range of annealing procedures were investigated to maximize the ductility of each alloy. Both alloy wires underwent annealing between 250 and 450 °C for soak times between 10 and 120 min. All annealing procedures were carried out using a modified tube furnace that allowed for rapid heating and cooling of the samples under vacuum conditions to prevent oxidation.

2.2. Microstructural Characterization

Investigation of the wires’ microstructure was performed on cross sections in the normal direction, using optical microscopy, scanning electron microscopy (SEM), energy-dispersive spectroscopy (EDS), and electron backscatter diffraction (EBSD). Samples analyzed using optical microscopy were mounted in epoxy resin and mechanically ground and polished using 1200 and 2400 grit silicon carbide paper followed by polishing with colloidal silica and etched with a solution of 75 mL of ethylene glycol, 10 mL distilled water, and 1 mL of nitric acid. Samples for SEM and EDS analysis were mounted and prepared with the same method as above without the etching process. Images were taken using the backscatter electron (BSE) detector. To enhance conductivity, a thin layer (≈10 nm) of gold was deposited on the surface prior to analysis. Samples for EBSD analysis were mounted in conducting Bakelite and prepared with the same methods as above, without the etching process, followed by ion milling with a Gatan precision etching and coating system. EBSD analysis was carried out on a 50 × 50 μm area in the center of the cross section of the wires using a step size of 0.1 μm, with a JEOL 7900 F field emission gun SEM.

X-ray diffraction (XRD) (Bruker D8 Advance) was carried out for phase identification. The XRD analysis used Cu Kα radiation (λ = 1.5406 Å) with an acceleration voltage of 45 kV, current of 40 mA, step size of 0.0025°, step time of 0.1 s, and a 2θ range of 10–90°.

2.3. Mechanical Testing

Vickers microhardness tests were conducted on both alloy wires in their cold drawn and annealed states. It is generally accepted that during cold drawing, the regions of wire furthest from the center undergo increased deformation compared to regions closer to the center. This commonly results in increased hardness and internal stress of the regions furthest from the

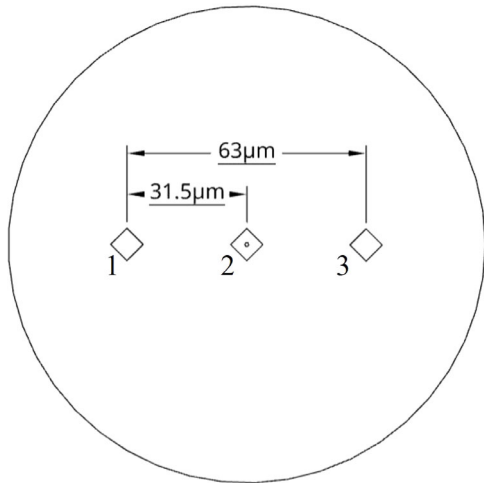


Figure 1. Indent locations on the cross sections of the wire.

center.^[6,33] Samples were mounted in epoxy resin and mechanically ground and polished following the same procedure as described for optical microscopy, without the final etching step. Microhardness measurements (0.003 Hv) were taken at three locations through the cross sections (**Figure 1**). The data from point 2 was used to determine the hardness in the center of the wire, and the data from points 1 and 3 were collated and used to determine the hardness of the wire midway between the center and OD, from here referred to as the mid-radial position. The center point (point 2) of each sample was measured first, then the samples were reground and polished before indents 1 and 3 were measured. A total of 12 samples were analyzed per wire condition and, to improve accuracy, the maximum and minimum values were removed from each data set.

To determine the mechanical behavior of the wire, tensile tests were performed using an Instron 4442 equipped with a 100 N load cell and capstan style grips. A sample size of 5 was used for each processing condition. A gauge length of 110 mm and a cross head speed of 6.6 mm min^{-1} (corresponding to an initial strain rate of 0.001 s^{-1}) were used for each test.

Minimum bend diameter (MBD) tests were carried out by wrapping each wire around a series of small diameter pins

(<0.3 mm diameter), according to the ISO 7802:2013 standard.^[34] Successful tests were defined by whether the wire could be successfully wrapped at least five times around the pin without failure. Three wrapping tests were performed for each pin size, and post testing samples were checked to ensure that each consecutive wrapped diameter was in contact with the previous. During wrapping tests, the wire was held tight using a 0.01 kg mass (<5% of the tensile strength as specified by the ISO 7802:2013 standard).^[34]

3. Results and Discussion

3.1. Microstructure

The microstructure of the as-drawn alloy wires in the normal direction both exhibits a typical deformed structure with no visible equiaxed grains (**Figure 2**). After annealing for 10 min at 250 °C, equiaxed grains are developed near the OD of the 0.5Y alloy wire (**Figure 3a,c**). No recrystallized grains are developed in the center of the wire when annealed under these conditions (**Figure 3b**). The 2Y alloy wire required a higher temperature (300 °C) for equiaxed grains to begin forming near the OD after 10 min of annealing (**Figure 3f**). The center of the 2Y wire remained unrecrystallized under these conditions. Evolution of the microstructure of the 0.5Y and 2Y wires when treated at 250 and 300 °C, respectively, for prolonged soak times was investigated through analysis of $50 \times 50 \mu\text{m}$ areas in the center of each wire cross section (**Figure 4**). Equiaxed grains begin to form and progress into the center of the 0.5Y wire following annealing at 250 °C for 20 min, though there remains an unrecrystallized region in the center of the wire. Equiaxed grains are formed throughout the 0.5Y wires cross section after annealing for 30 min (**Figure 4a2**), though the grains in the center of the wire are smaller compared to surrounding areas closer to the OD, suggesting recrystallization is complete but little growth has occurred. As the soak temperature is increased, a more uniform grain size distribution is formed through the cross section of the 0.5Y wire (**Figure 4a3 and a4**). Accurate grain size measurements for select samples were conducted using EBSD analysis (Section 3.3). After annealing for 20 min at 300 °C, equiaxed grains are seen to develop throughout the full cross section of the

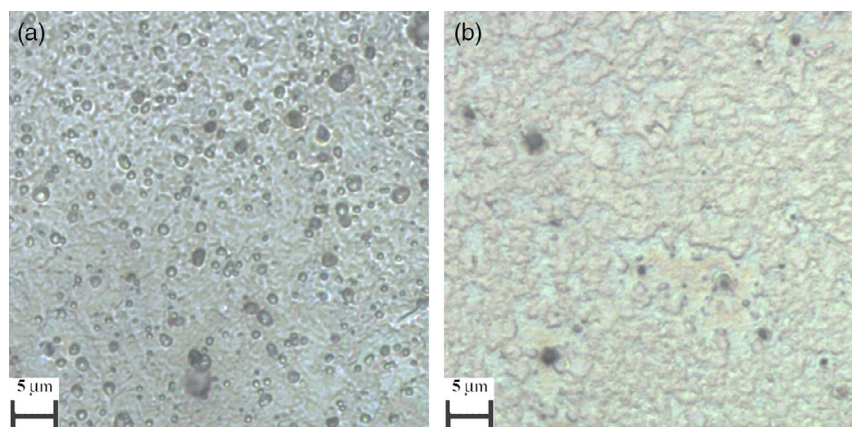


Figure 2. Microstructure of cold drawn alloy wires a) 0.5Y. b) 2Y.

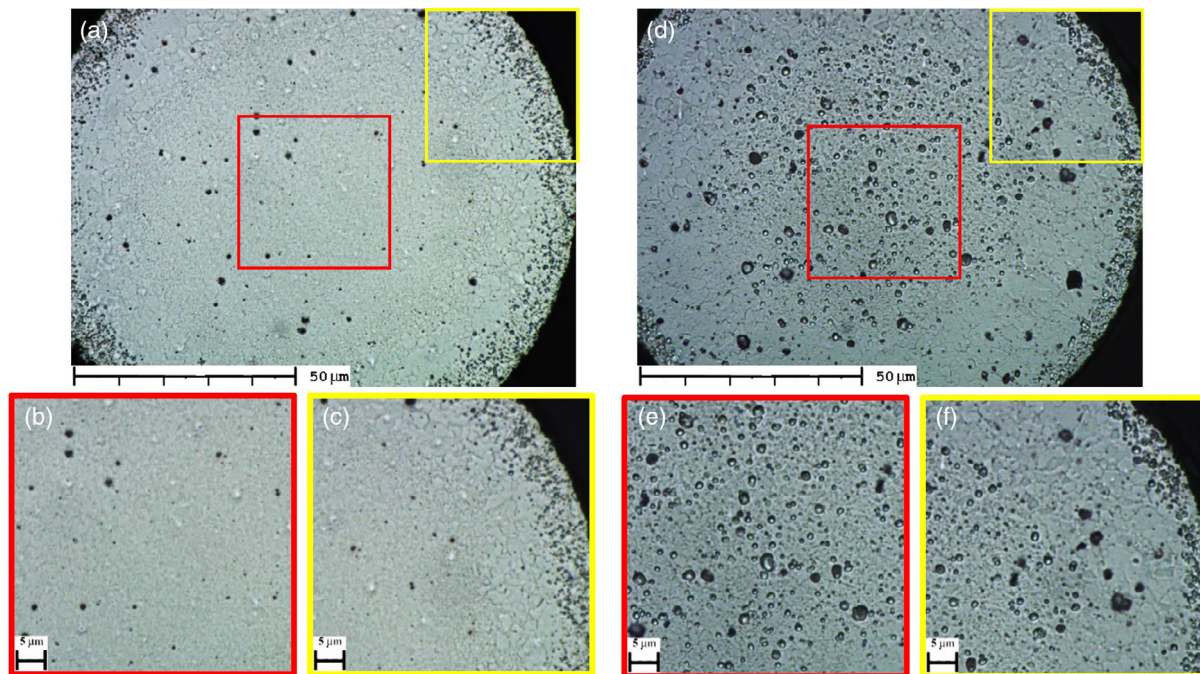


Figure 3. Microstructure of 0.5Y wire annealed at 250 °C for 10 min a) full cross section. b) center. c) OD and 2Y wire annealed at 300 °C for 10 min. d) full cross section. e) center. f) OD.

2Y alloy wire with a homogeneous grain size. Little change is seen in the grain size as the soak time is increased in the 2Y alloy wire. During cold drawing, the regions closest to the OD of the wire undergo increased deformation, resulting in increased internal stress that acts as a driving force for nucleation, hence equiaxed grains are first developed around the OD of both alloy wires during annealing. As soak time or temperature increases, the regions of the wire closer to the center begin to recrystallize and grow new grains. Blocky secondary phase particles are observed in each alloy's microstructure (an example in each image in Figure 4 is identified with a black arrow), and the number and size of these particles precipitated out of solution increase in both alloy wires with soak time. SEM/EDS analysis was carried out on the 0.5Y and 2Y alloy wires following annealing for 30 min at 250 °C and 20 min at 300 °C, respectively, to investigate the distribution of secondary phases in the wires upon complete recrystallization (Figure 5). Areas with a higher concentration of Y will appear bright compared to the Mg matrix using the BSE detector. The small cubic particles observed in optical microscopy are also apparent in Figure 5a,b and appear brighter compared to the Mg matrix, indicating they contain higher concentrations of Y than the bulk Mg matrix. Figure 5a,b each include an inset higher magnification SEM image which show such particles. EDS analysis of these particles estimated the Y content to be 36.4 and 31.7 at% for the 0.5 and 2Y alloys, respectively (Figure 5c,d). As expected, owing to the higher Y content of the 2Y alloy wire, there are an increased number of Y-rich secondary phase particles distributed throughout the 2Y wires cross section following complete recrystallization compared to the 0.5Y alloy wire.

Investigation of the microstructure of the 0.5Y and 2Y alloy wires at higher soak temperatures of 350, 400, and 450 °C

(Figure 6 and 7, respectively) demonstrated that grain coarsening of the 0.5Y occurred during annealing, while little grain growth was observed in the 2Y alloy during prolonged annealing. Upon complete recrystallization, the 2Y alloy wire contained an increased number of precipitates (Figure 5) that will act to restrict boundary mobility during prolonged annealing. A large number of precipitates are also developed in the 0.5Y alloy (Figure 6) that might be expected to restrict boundary mobility. However, it is shown that these particles develop following complete recrystallization and grain coarsening is already underway and as such these particles are shown to not promote recrystallization of a more homogeneous microstructure. Further, Y and other RE elements are known to segregate to grain boundaries, restricting their mobility during thermal processing that can promote texture weakening and recrystallization of a more homogenous microstructure.^[35,36] It is shown that increasing the Y content to 2 wt% develops a more homogeneous microstructure and prevents grain coarsening during annealing at higher temperatures, either through particle pinning, solute drag, or some combination of both. Precipitation of secondary phase particles increased in both alloys as both soak time and temperature increased. Generally, low temperatures (200–300 °C) are used to develop precipitates in Mg alloys, and fewer particles are developed at elevated temperatures (e.g., >400 °C). However, Guan et al.^[20] reported a similar phenomenon in WE43, whereby concurrent precipitation and recrystallization were observed during high-temperature annealing (490 °C), suggesting it was caused by a combination of high residual strain and high solute concentration along prior grain and twin boundaries.^[20] Both wires investigated here have been severely cold drawn and as such will have high residual strain prior to annealing, while microstructural analysis observed few particles were present in both cold

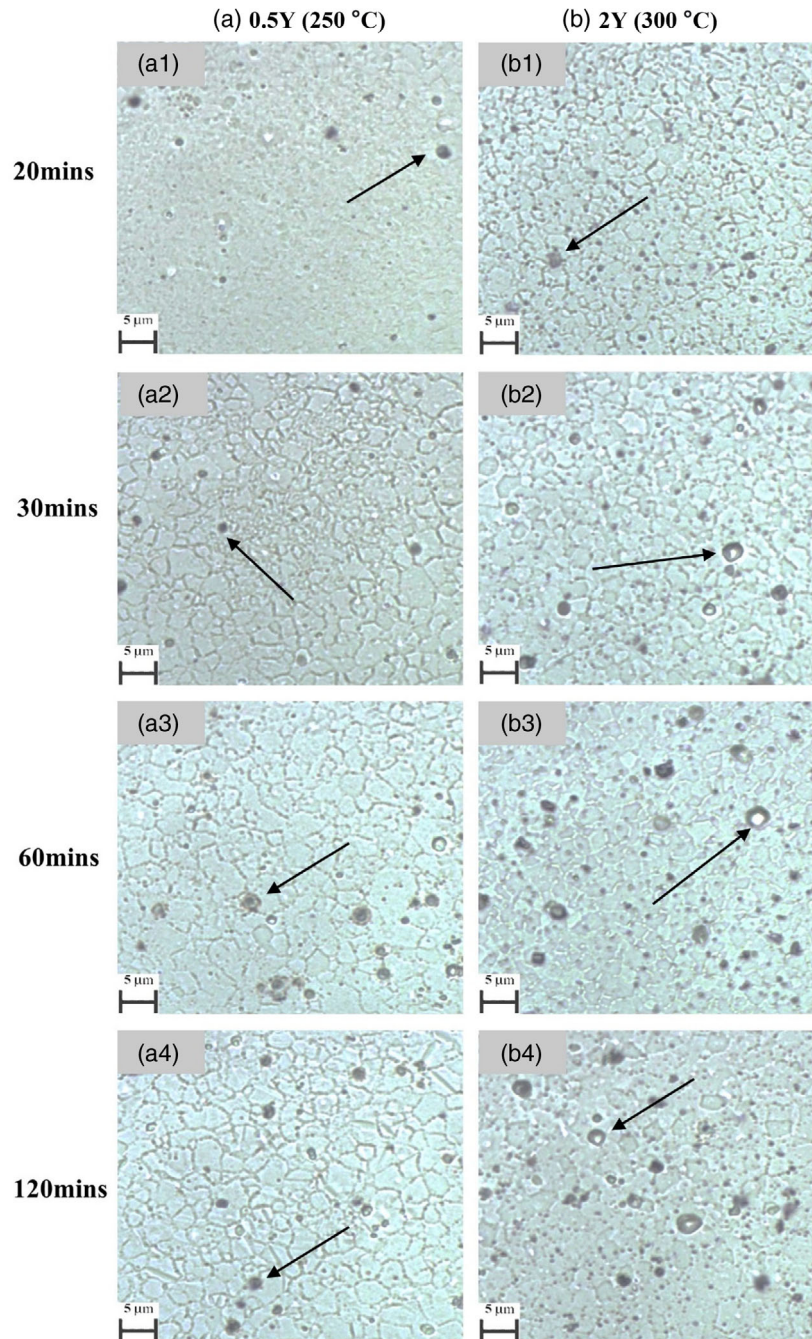


Figure 4. Annealed microstructures of both alloys over a range of soak temperatures, and arrows highlight secondary phase particles a) 0.5Y. b) 2Y.

drawn wires meaning the alloys analyzed here have similar characteristics to those investigated by Guan et al. The particles developed were Y-rich, and estimates can be made on the composition of these particles based on the EDS analysis; however, XRD analysis (**Figure 8**) was used to identify the true composition. The XRD analysis identified these particles as $Mg_{24}Y_5$. No Li-rich secondary phase was identified in the XRD analysis demonstrating that the Li was maintained in solid solution, as expected when the Li content is below 5.5 wt%.

3.2. Mechanical Properties

Microhardness tests were conducted on the 0.5Y and 2Y wires in their cold drawn state and when annealed at 250 and 300 °C (**Figure 9**—where zero on the Time axis represents the cold drawn state). Both cold drawn wires have increased hardness at their mid-radial positions compared to their centers. The 0.5Y and 2Y wires have a hardness of 87.1 ± 2.7 and 88.6 ± 1.4 Hv, respectively, at the center of their cross sections.

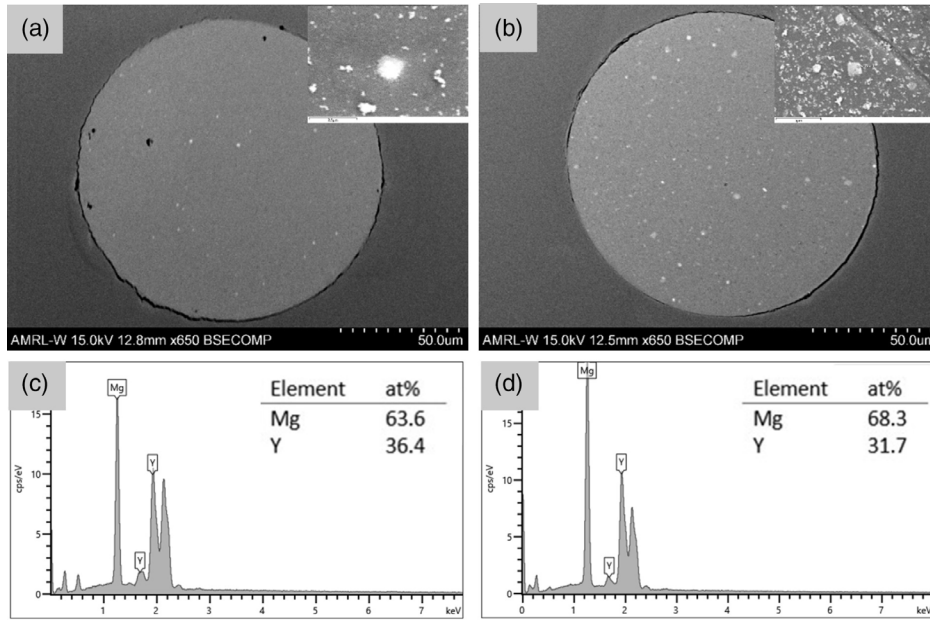


Figure 5. BSE images of wire cross sections with zoomed in SEM image of representative secondary phase particle analyzed with EDS a) 0.5Y wire annealed at 250 °C for 30 min. b) 2Y wire annealed at 300 °C for 20 min. EDS spectra of representative secondary phase particle from c) 0.5Y wire annealed at 250 °C for 30 min d) 2Y wire annealed at 300 °C for 20 min.

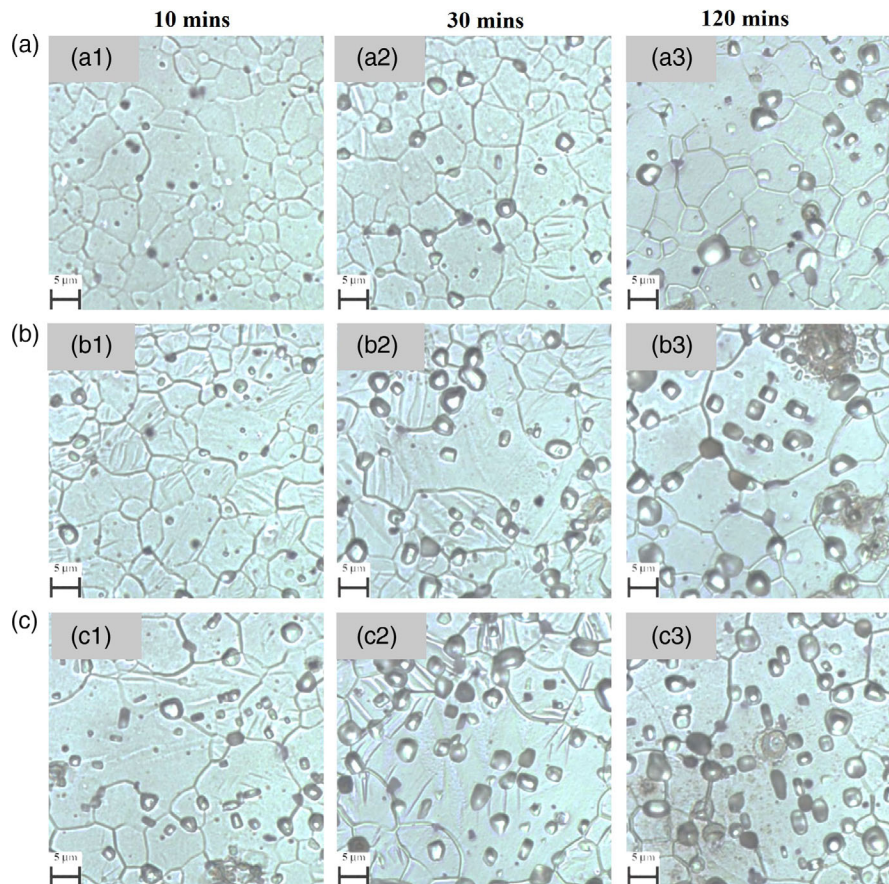


Figure 6. 0.5Y wire microstructures annealed at different temperatures for 10, 30, and 120 min a) 350 °C. b) 400 °C. c) 450 °C.

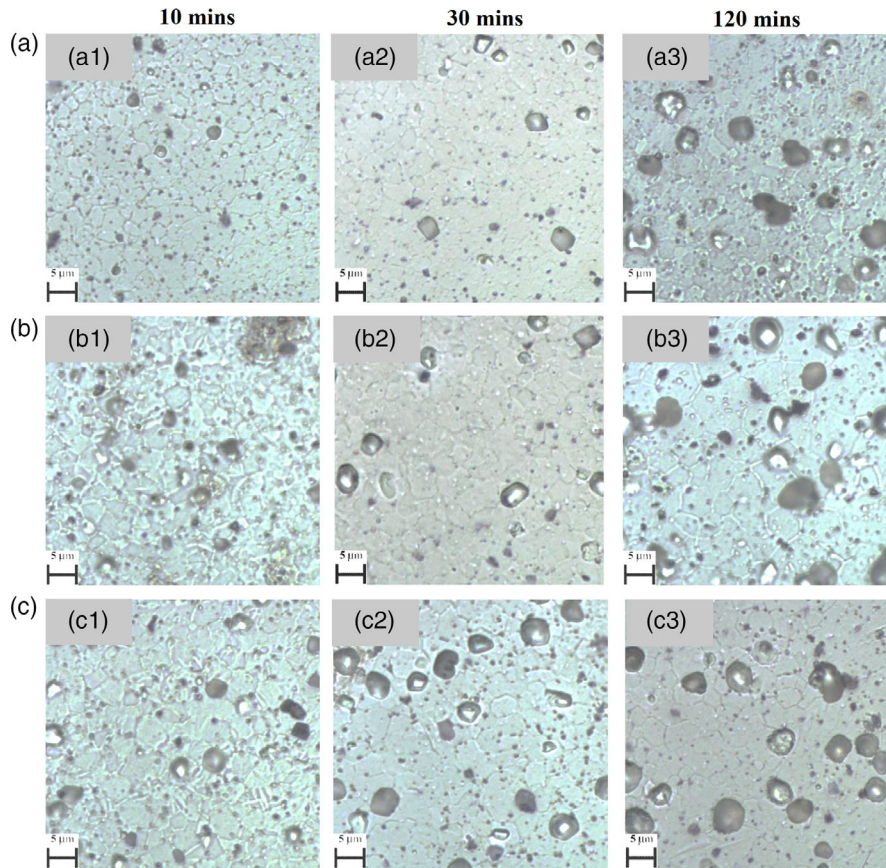


Figure 7. 2Y wire microstructures annealed at different temperatures for 10, 30, and 120 min a) 350 °C. b) 400 °C. c) 450 °C.

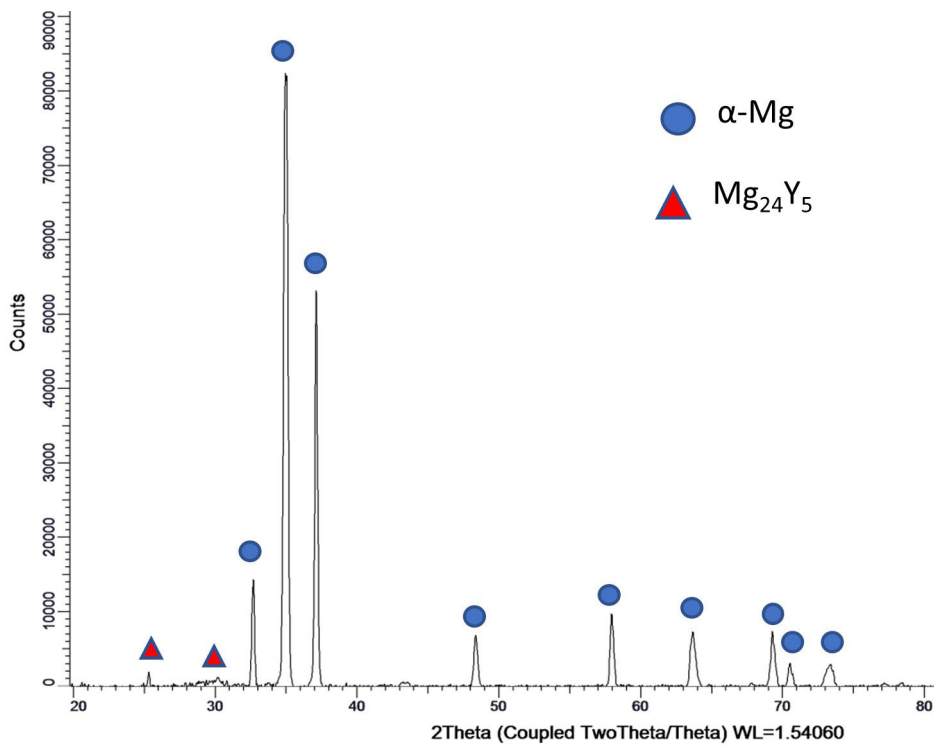


Figure 8. XRD spectrum of 0.5Y wire annealed at 450 °C 30 min.

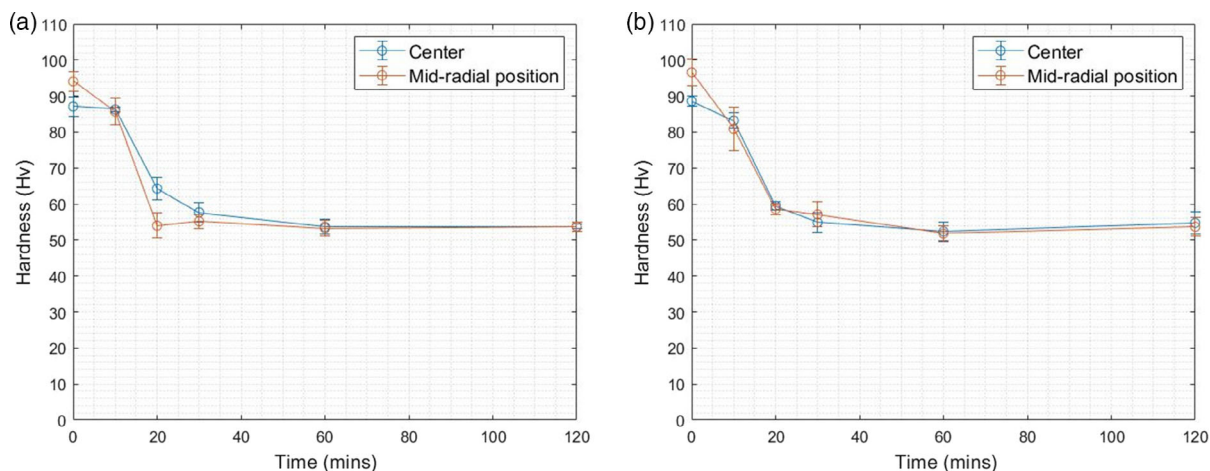


Figure 9. Microhardness values at the center and mid-radial position of each alloy wire a) 0.5Y wire annealed at 250 °C. b) 2Y wire annealed at 300 °C. Error bars show standard deviation.

At the mid-radial position, the hardness of the 0.5Y and 2Y wires was found to be 94.1 ± 2.7 and 96.6 ± 3.8 Hv, respectively. This hardness distribution is attributed to the regions of the wire furthest from the center undergoing increased deformation, confirming why recrystallization is seen to initiate first from the regions of increased hardness/internal stress at the OD of the wire. As recrystallization progresses in both alloys, the hardness at both the center and mid-radial positions follows a similar trend: rapidly decreasing as soak time is increased from 0 to 30 min and subsequently stabilizing in the range 50–54 Hv as soak time is increased to 120 min. In both alloys, the hardness at the mid-radial position of the wire decreases at a faster rate compared to the center, which is attributed to recrystallization initiating first at the OD and progressing inwards.

Representative stress–strain plots of the two wires in their cold drawn state are shown in **Figure 10**. The cold drawn 0.5Y wire exhibits relatively high strength (yield strength (YS)

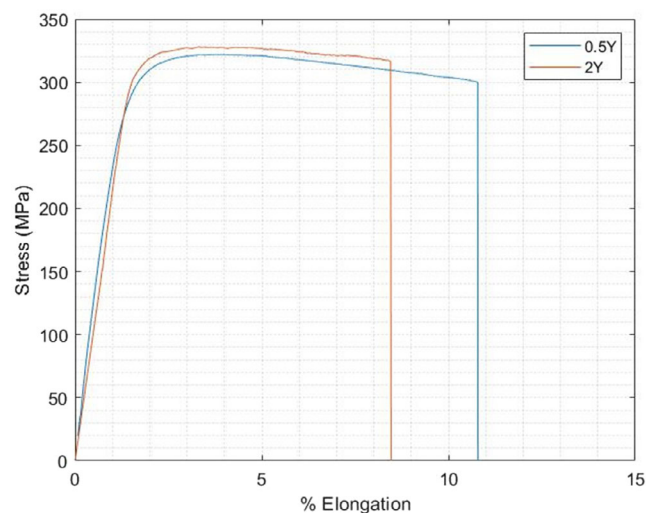


Figure 10. Representative stress strain plots of the cold drawn wire.

271 \pm 7.0 MPa and ultimate tensile strength (UTS) 322 \pm 0.4 MPa) and elongation (11.8 \pm 1.0%) for cold drawn Mg wires. The 2Y wire has slightly higher YS (302 \pm 8.2 MPa) but similar UTS (327 \pm 3.6 MPa) and reduced elongation (8.4 \pm 2.5%) compared to the 0.5Y wire.

The mechanical properties of both wires following the range of annealing treatments are plotted in **Figure 11**. The 0.5Y wire is not fully recrystallized when annealed at 250 °C for 10 min, which is reflected in the mechanical properties as the YS and UTS remain relatively high, 200 \pm 3.1 and 250 \pm 0.4 MPa, respectively, while the elongation to failure is 8.9 \pm 0.3%. The microstructural investigation revealed that a fully recrystallized microstructure developed following annealing at 250 °C for 30 min which resulted in maximized elongation to failure of 20.3 \pm 0.4%, while the YS and UTS fall to 133 \pm 2.6 and 196 \pm 0.8 MPa, respectively. These properties remain relatively consistent as the soak time is increased further at 250 °C, showing that no increase in ductility was achieved as a more homogeneous grain size distribution developed. At the higher soak temperatures, ductility is maximized after annealing for 10 or 20 min and follows a downward trend with increasing soak time. When treated at 400 and 450 °C, there is a general upward trend in YS as soak time progresses (the 450 °C at 120 min YS point was not plotted because it fractures before yield). In all of the 400 and 450 °C samples, ductility is severely reduced, and they fail soon after yield (except the sample treated at 450 °C for 120 min) meaning the upward trend is not as visible in the UTS values as little strain hardening takes place. The increased strength at higher soak temperatures is attributed to increased precipitation of Mg₂₄Y₅ particles, while the reduced ductility is attributed to both the increased precipitation and grain coarsening.

The 2Y wire displays a similar trend to the 0.5Y wire, though as shown in the microstructural analysis, increased temperature and/or soak time is required to fully recrystallize the microstructure. When treated at 250 °C the wire exhibits relatively high strength and low ductility until prolonged annealing for 120 min where the YS and UTS fall to 146 \pm 0.7 and

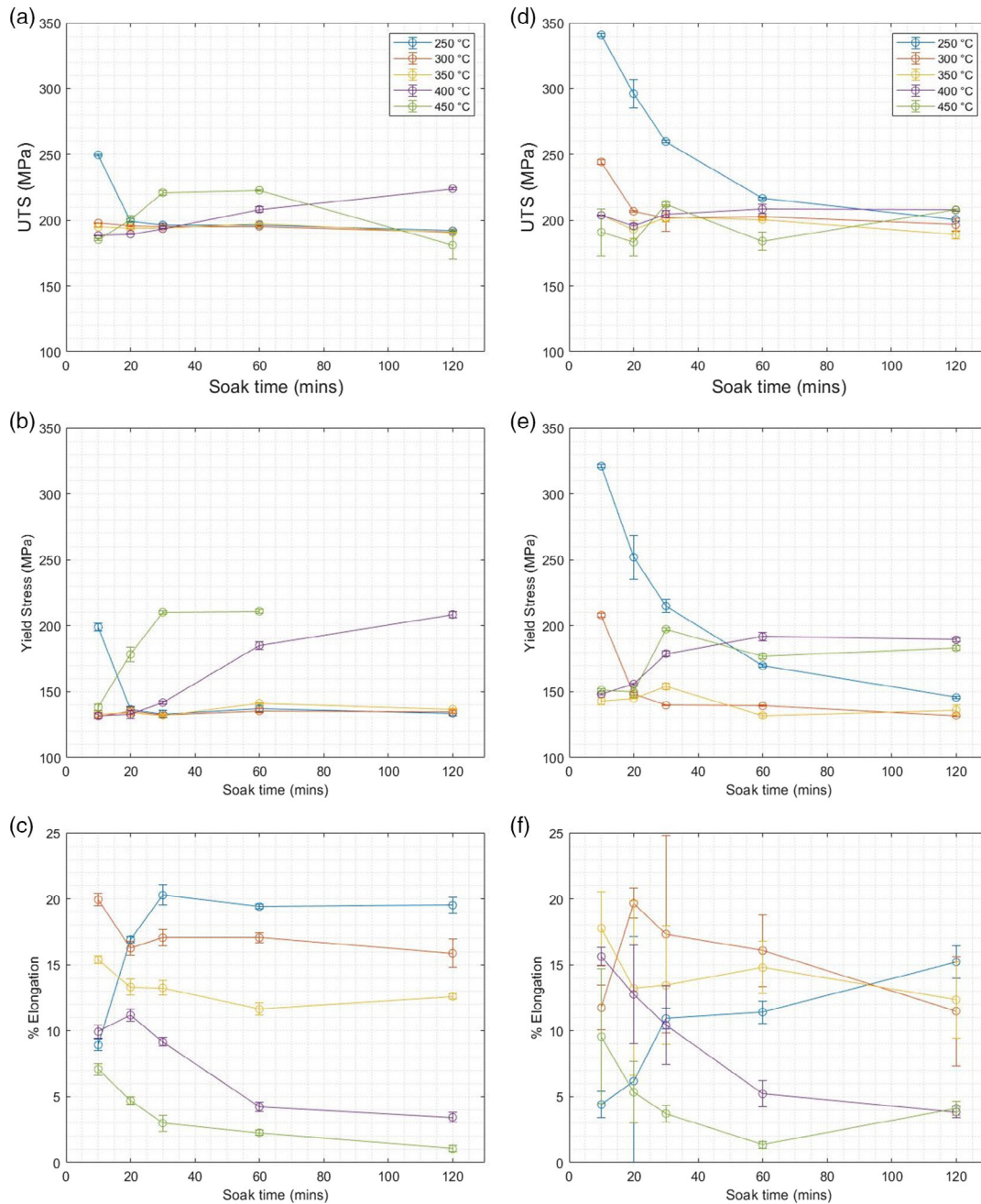


Figure 11. Mechanical properties of both alloys post annealing a) 0.5Y UTS. b) 0.5Y YS. c) 0.5Y % Elongation to failure. d) 2Y UTS. e) 2Y YS. f) 2Y % Elongation to failure. Error bars show standard deviation.

201 ± 1.2 MPa, respectively, while the elongation to failure is 15.2 ± 5.6%. A fully recrystallized microstructure is developed when treated at 300 °C for 20 min resulting in a maximized elongation to failure of 19.7 ± 1.1%. As the soak time is increased at 300 °C, increased precipitation was observed (Figure 4) and consequently the elongation to failure decreases. As in the 0.5Y wire, strengthening and loss of ductility are seen during annealing at high temperatures (400 and 450 °C) with long soak times. As the grain size remains relatively constant as soak time and

temperature are increased, this loss of ductility is attributed solely to the increased precipitation of Mg₂₄Y₅ particles in the 2Y alloy wire.

For the purpose of this study, it was required to select an individual annealing process that would be termed “optimum” for each alloy wire and used for further mechanical and microstructural analysis. For the 0.5Y alloy wire, the process selected was 250 °C for 30 min where the elongation to failure, YS and UTS were 20.3 ± 0.4%, 133 ± 2.6 MPa, and 196 ± 0.8 MPa,

respectively. For the 2Y wire, the optimum process selected was when annealed at 300 °C for 20 min where the elongation to failure, YS, and UTS were $19.7 \pm 1.1\%$, 150 ± 2.0 MPa, and 207 ± 0.4 MPa, respectively. Increasing the Y content from 0.5 to 2.0 wt% has little effect on the maximum achievable tensile elongation of the two alloy wires; however, both the YS and UTS of the wires increase by approximately 20 and 10 MPa, respectively.

To further investigate each wire's suitability for use in medical devices where they will undergo more complex loading, wrapping tests were carried out on the wires in their optimum conditions post heat treatment as well as in their cold drawn state. The wrapping tests were limited in that the smallest wrapping diameter tested was 0.135 mm. All wires tested were shown to survive wrapping around this diameter other than the 2Y cold drawn wire which failed during one of the three tests carried out (Figure 12). Repeat testing at larger wrapping diameters found the MBD of the 2Y cold drawn wire to be 0.16 mm. The corresponding maximum idealized bending strains on the surface of the wire at 0.135 and 0.16 mm wrapping diameters are 48 and 44%, respectively. Wrapping tests were not carried out at lower diameters due to the complex nature of wrapping such fine wire around small diameters, meaning the two annealed alloys could not be distinguished from one another in terms of MBD. Proof that both alloy wires can survive wrapping around such small diameters supports their suitability for application in complex wire form medical devices as both can undergo considerable bending strains that are higher than similar Mg alloy wires.^[10,37]

3.3. Texture

EBSD analysis of a $50 \times 50 \mu\text{m}$ area in the center of the wire was carried out on samples of both alloy wires following annealing. Analysis of both cold drawn wires output no useable data owing to the high dislocation density developed during cold drawing. The inverse pole figure (IPF) maps are shown Figure 13, it should be noted that drift during scanning of the 2Y wire annealed at 350 °C for 20 min (Figure 13e) resulted in a $50 \times 40 \mu\text{m}$ area being analyzed. Despite no quantification of the texture of the two cold drawn wires, it is considered that they both exhibit a basal fibre texture, commonly associated with cold drawn magnesium wires.^[8,10]

The IPF maps in Figure 13a,d show the microstructure of the 0.5Y and 2Y alloy wires when annealed for maximum ductility. The uneven grain size distribution in the 0.5Y alloy wire treated at 250 °C for 30 min is shown more clearly here compared to the optical micrographs. Figure 14 highlights the central region (Figure 14a) and edge of the map (Figure 14b) where the mean grain size has been calculated as 1.18 and 2.12 μm , respectively. The full map has a mean grain size of 1.87 μm . As grain growth progresses in the 0.5Y samples annealed at higher temperatures, coarsening of some grains takes place. In the sample treated at 350 °C, the mean grain size increases to 6.4 μm , and in the sample treated at 450 °C, one grain with a diameter of $\approx 30 \mu\text{m}$ dominates the IPF map. A more uniform grain size distribution is developed in the 2Y alloy wire post annealing at all temperatures analyzed, with the samples treated at 300, 350, and 400 °C grain sizes being 2.48, 2.57, and 2.68 μm , respectively.

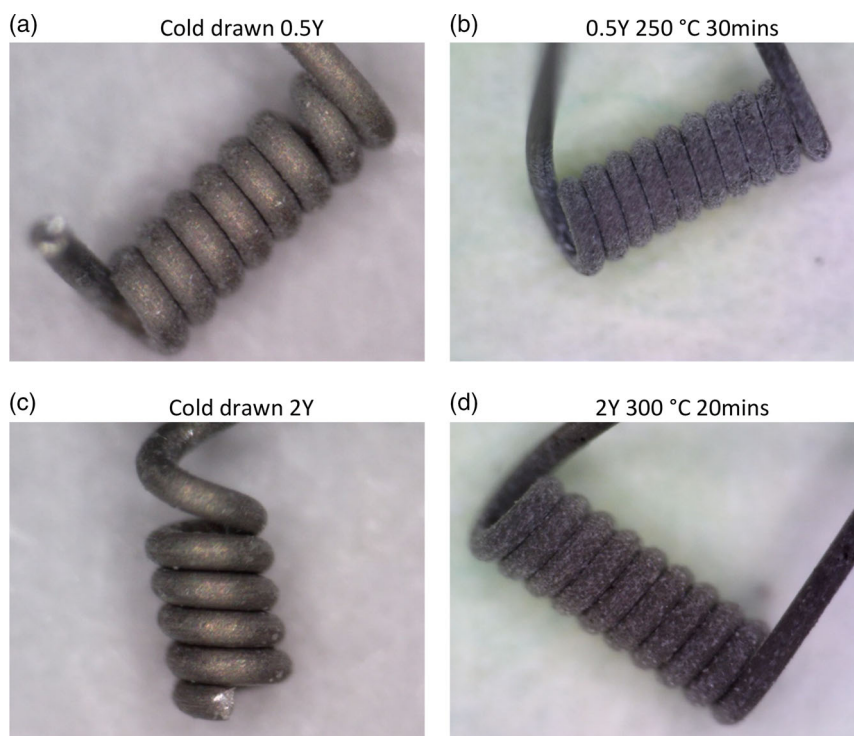


Figure 12. MBD test results for wrapping diameters of 0.135 mm a) cold drawn 0.5Y b) 0.5Y 250 °C 30 min c) cold drawn 2Y d) 2Y 300 °C 20 min.

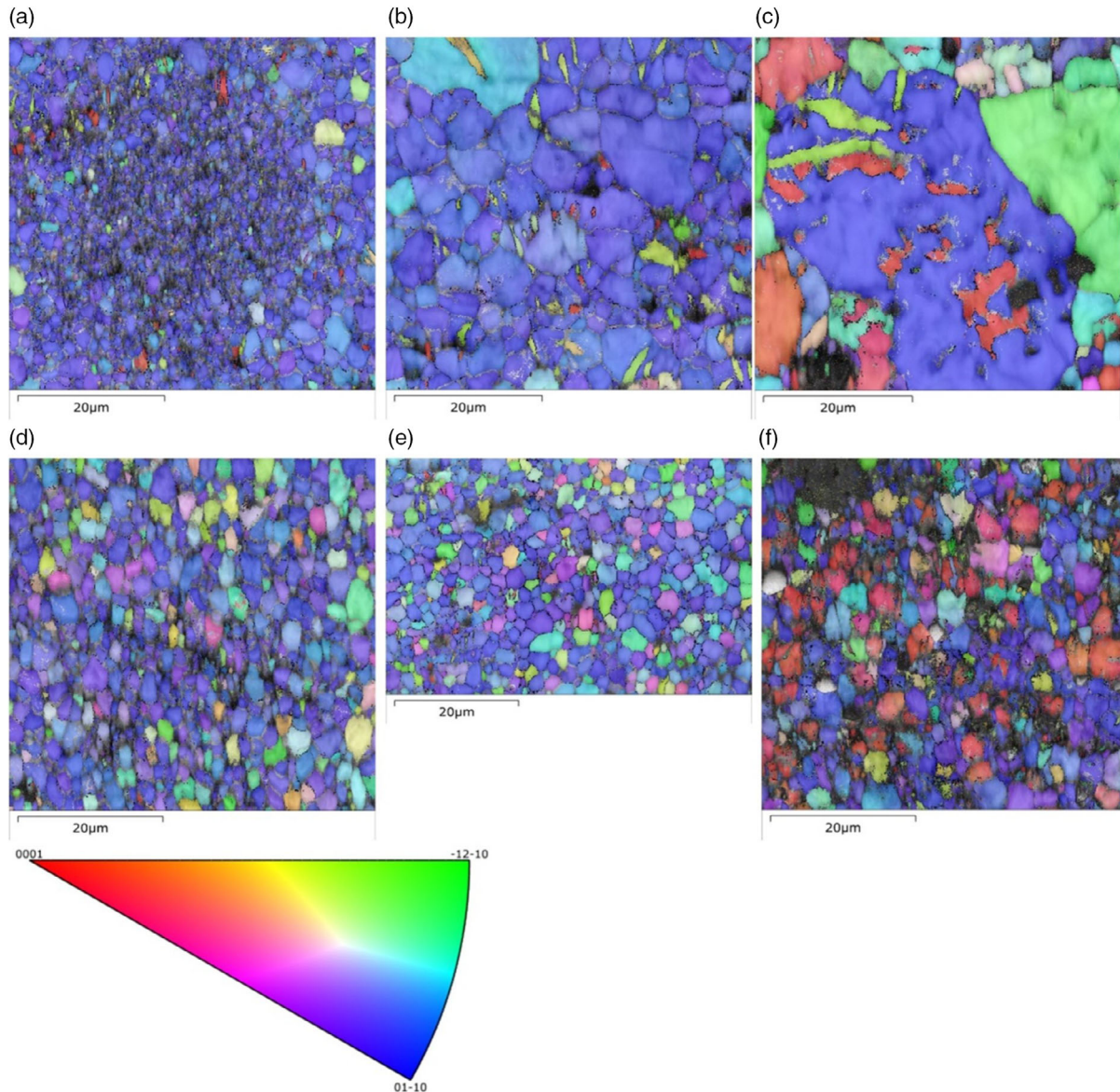


Figure 13. Inverse pole figure maps of both alloys post annealing a) 0.5Y 250 °C 30 min. b) 0.5Y 350 °C 30 min. c) 0.5Y 450 °C 30 min. d) 2Y 300 °C 20 min. e) 2Y 350 °C 20 min. f) 2Y 450 °C 20 min.

Figure 15 and **16** show the corresponding pole figures for the 0.5Y and 2Y wires, respectively. The pole figures for the 0.5Y wire show that the basal texture is maintained throughout the samples treated at 250 and 350 °C, where the (10 $\bar{1}$ 0) plane is perpendicular to the DD, and the (0001) plane lies parallel to the DD. The large grain in the IPF map for the 0.5Y wire treated at 450 °C for 30 min dominates the microstructure causing a very strong texture in the corresponding pole figures (Figure 15c), particularly in the (0001) pole figure. As only a 50 × 50 μm region has been analyzed in this sample, the large grain dominated the analysis and results in a very high texture intensity, if a larger region with increased number of grains were analyzed, it is expected that the texture intensity would decrease. A similar effect is observed in the wire treated at 350 °C, owing to the increased grain size

relative to the sample treated at 250 °C for 30 min, though to a lesser extent.

The 2Y alloy wire develops a basal texture when treated at 300 and 350 °C, but the intensities are lower than that of the 0.5Y alloy wire (Figure 16). A rotation of the (0001) plane is observed in the sample treated at 400 °C for 20 min. The (0001) plane reorients by approximately 87°, which would be expected in an Mg alloy with extension twinning present; however, there are no clear twins in the microstructure (Figure 13f). A large number of precipitates were present post annealing in the 2Y alloy wire annealed at 400 °C for 20 min; however, from the analysis carried out here, it is unclear if the precipitation occurred pre, post, or concurrently with recrystallization. Depending on the sequence of precipitation and recrystallization, this texture may be better

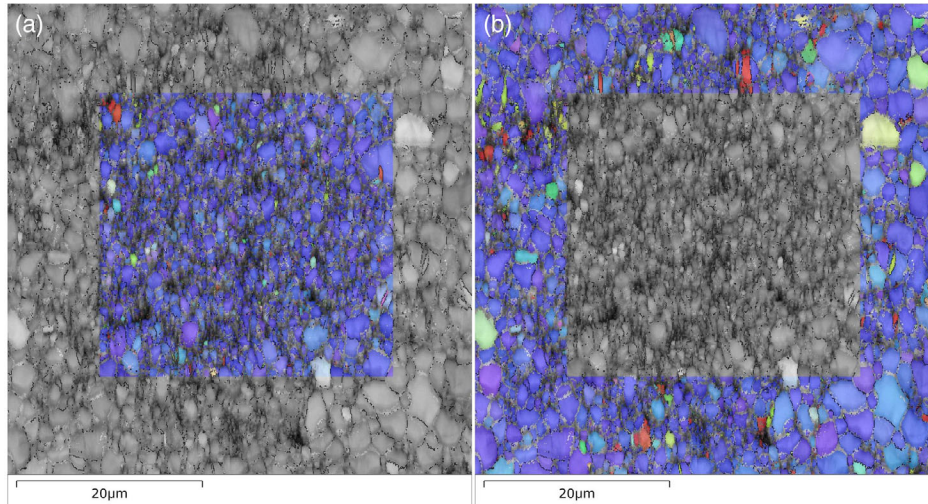


Figure 14. IPF maps of 0.5Y wire annealed at 250 °C for 30 min a) Center of map/wire. b) Edge of map/area closer to the OD.

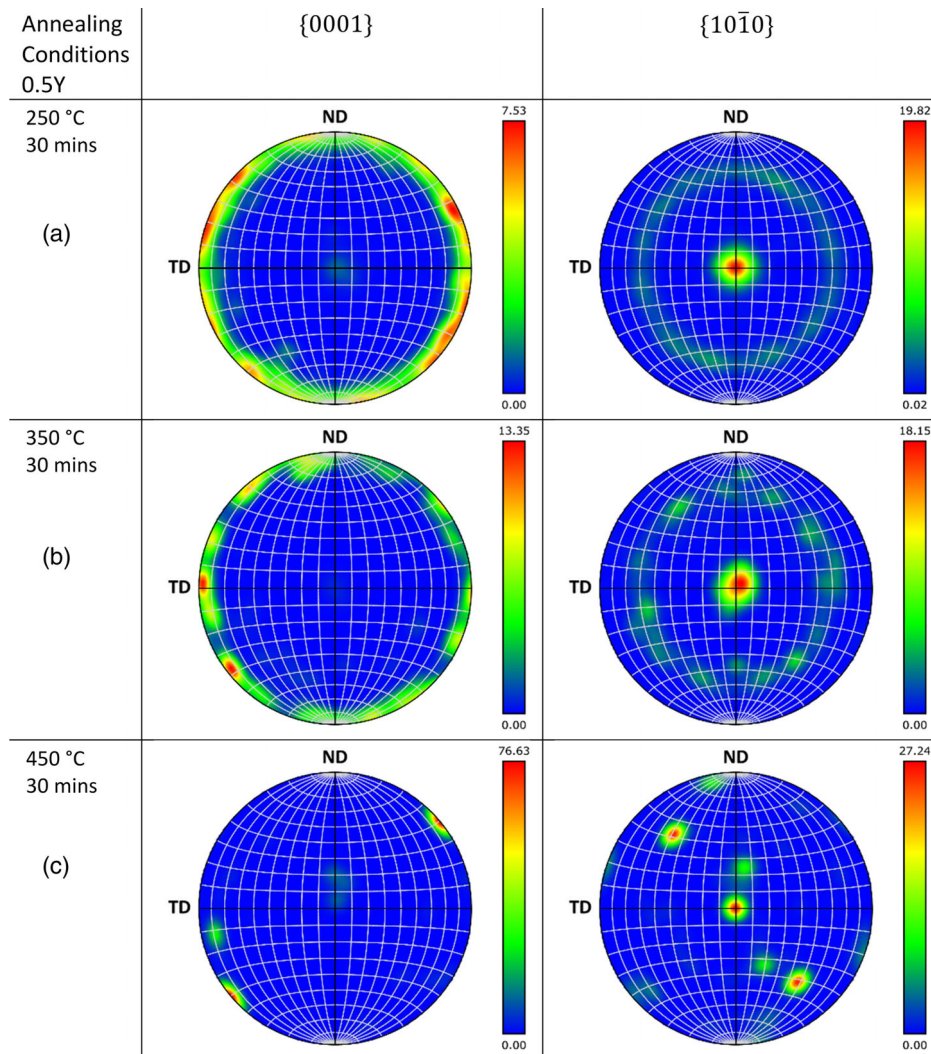


Figure 15. Pole figures of 0.5Y alloy wires post annealing.

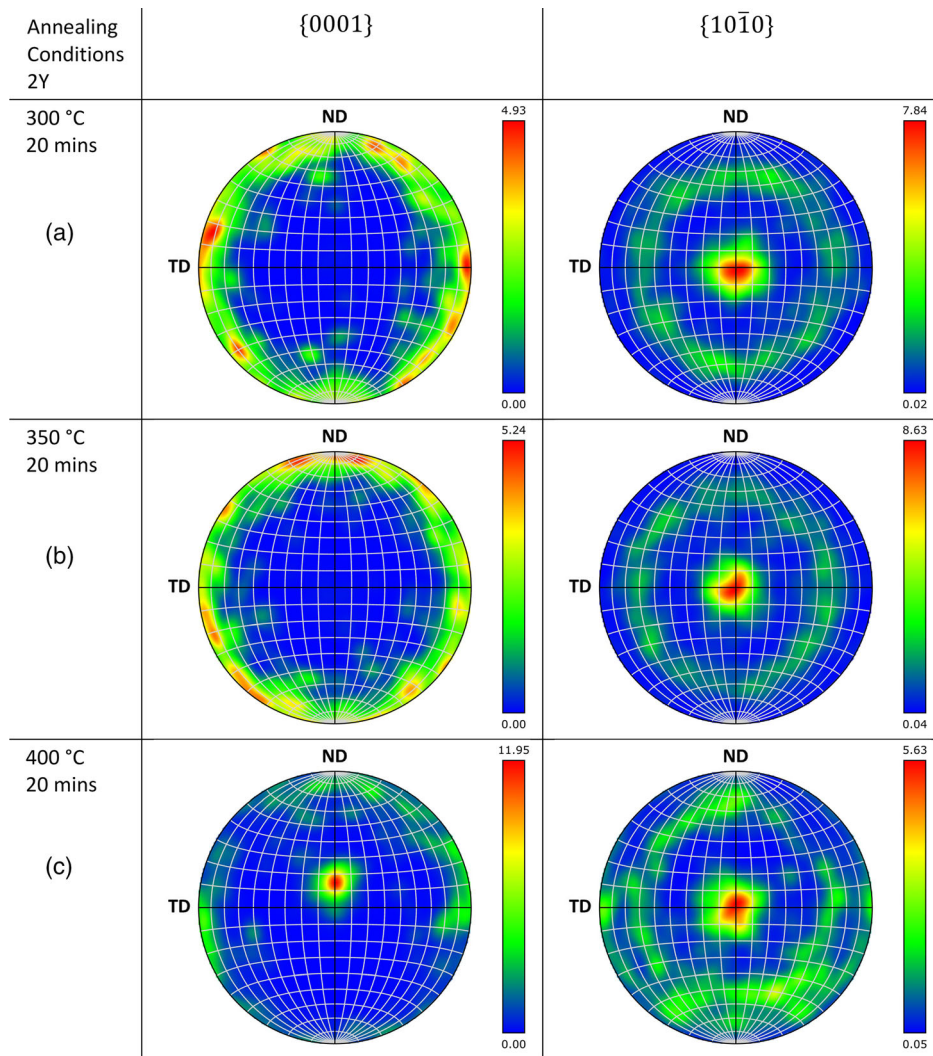


Figure 16. Pole figures for 2Y alloys wires post annealing.

understood as the precipitates could be affecting the recrystallization mechanisms activated or grain growth post nucleation.

Both alloy wires retain a transverse basal texture post annealing, when treated for maximum ductility, which is common with similar MgRE alloy wires.^[10,29,38] There is a distinct difference in intensities between the two alloys whereby the 2Y alloy develops a weaker texture post annealing compared to the 0.5Y alloy. It is known that a minimum level of RE elements are required to activate texture weakening. From the results shown here, it would suggest that the 0.5Y alloy wire has insufficient Y content to activate texture weakening. Hantzsche et al.^[27] concluded that an Y content of greater than 0.17 at% is required to activate texture weakening in MgY alloys. The 0.5Y and 2Y alloys investigated here contain 0.12 and 0.50 at% Y, respectively, agreeing with the work of Hantzsche et al.^[27] that there is insufficient Y content in the 0.5Y alloy to activate texture weakening. Despite the weaker texture in the 2Y sample post annealing at 300 °C for 20 min, it still exhibits similar ductility to the 0.5Y alloy wire. Though the ductility of the two alloys is comparable, there may be some improvement in the 2Y wires bending behavior,

owing to the weakened basal texture, compared to the 0.5Y alloy. The MBD tests were limited in that the minimum wrapping diameter tested was 0.135 mm which was not sufficient in distinguishing between the 0.5Y and 2Y alloy wires when heat treated for maximum tensile elongation. If smaller bend diameters could be tested, the 2Y alloy wire may be shown to have a smaller MBD than the 0.5Y wire, due to the weakened basal texture. If no true difference in formability of the wires can be identified, then the 0.5Y alloy wire may prove to be preferable, owing to the lower Y content, for application in medical devices. If, however, the weakened basal texture developed in the 2Y alloy wire is shown to be beneficial, then the Y content could be minimized to be closer to the limiting range for texture weakening (0.17 at%/0.62 wt%) in Y-containing alloys.

4. Conclusion

The microstructure and mechanical properties of two Mg–Li–Y alloy wires were investigated in their as-drawn state, and an

annealing optimization process was developed and carried out on each to maximize their ductility. Recrystallization was seen to initiate near the OD of both alloy wires and progress to the center of the wire as soak time/temperature increased. The ductility of both wires was shown to be maximized soon after complete recrystallization and decreased with prolonged annealing. It was shown that the annealing the 0.5Y alloy wire at 250 °C for 30 min and the 2Y wire at 300 °C for 20 min maximized their elongation to failure. The reduction in ductility during prolonged anneals was attributed to increased number of secondary phase particles and grain coarsening in the 0.5Y alloy wire. Increasing the Y content to 2 wt% restricted grain coarsening during annealing at high soak temperatures and produced weaker textures compared to the 0.5Y alloy. Generally, it is assumed that more homogeneous microstructures with weaker textures are beneficial in increasing the ductility of Mg alloys, but this was not shown here. However, the weakened texture and more homogeneous microstructure of the 2Y alloy wire may reduce the anisotropy of the alloy and improve its performance under the complex loading a medical device is likely to experience. Both alloys are shown to exhibit high ductility following annealing under the optimized parameters indicating both are promising candidate materials for use in biomedical devices that undergo high levels of plastic deformation.

Acknowledgements

The authors wish to acknowledge the support of the Henry Royce Institute for advanced materials for (KM) through the Student Equipment Access Scheme enabling access to SEM/EBSD facilities at The Sorby Centre at the University of Sheffield; EPSRC Grant Number EP/R00661X/1. The original cold drawn wires were supplied by Fort Wayne Metals (USA).

Conflict of Interest

The authors declare no conflict of interest.

Data Availability Statement

The data that support the findings of this study are available from the corresponding author upon reasonable request.

Keywords

magnesium wires, mechanical property, microstructures, rare earth alloys, recrystallization

Received: August 11, 2022

Revised: November 25, 2022

Published online:

- [1] J.-M. Seitz, D. Utermöhlen, E. Wulf, C. Klose, F.-W. Bach, *Adv. Eng. Mater.* **2011**, *13*, 1087.
- [2] F. Witte, *Acta Biomater.* **2010**, *6*, 1680.
- [3] A. Chapuis, J. H. Driver, *Acta Mater.* **2011**, *59*, 1986.
- [4] J. Bai, L. Yin, Y. Lu, Y. Gan, F. Xue, C. Chu, J. Yan, K. Yan, X. Wan, Z. Tang, *Prog. Nat. Sci.* **2014**, *24*, 523.
- [5] J.-M. Seitz, M. Durisin, J. Goldman, J. W. Drelich, *Adv. Healthcare Mater.* **2015**, *4*, 1915.
- [6] H.-f. Sun, H.-y. Chao, E.-d. Wang, *Trans. Nonferrous Met. Soc. China* **2011**, *21*, s215.
- [7] L. Sun, J. Bai, L. Yin, Y. Gan, F. Xue, C. Chu, J. Yan, X. Wan, H. Ding, G. Zhou, *Mater. Sci. Eng., A* **2015**, *645*, 181.
- [8] M. Chatterton, J. Robson, D. Henry, *Texture Evolution During Wire Drawing of Mg-RE Alloy*, John Wiley & Sons, Inc, Hoboken, NJ, USA **2014**, pp. 251–256.
- [9] G. Chunlei, L. Xiaohui, N. Deng, Z. Xiang, Z. Kaihong, H. Zhenghua, in *IOP Conf. Series: Materials Science and Engineering*, IOP Publishing, Bristol, UK **2017**, p. 012051.
- [10] J. Xue, A. J. Griebel, Y. Zhang, C. Romany, B. Chen, J. Schaffer, T. P. Weihs, *Adv. Eng. Mater.* **2021**, *23*, 2001278.
- [11] A. J. Griebel, J. E. Schaffer, T. M. Hopkins, A. Alghalayini, T. Mkorombindo, K. O. Ojo, Z. Xu, K. J. Little, S. K. Pixley, *J. Biomed. Mater. Res. B Appl. Biomater.* **2018**, *106*, 1987.
- [12] A. A. Kaya, *Front. Mater.* **2020**, *7*, 198.
- [13] S. Tekumalla, S. Seetharaman, A. Almajid, M. Gupta, *Metals* **2015**, *5*, 1.
- [14] N. Hort, Y. Huang, D. Fechner, M. Störmer, C. Blawert, F. Witte, C. Vogt, H. Drücker, R. Willumeit, K. U. Kainer, F. Feyerabend, *Acta Biomater.* **2010**, *6*, 1714.
- [15] L. Duxue, Y. Donglin, L. Xinling, H. Shiwen, *J. Mater. Res. Technol.* **2019**, *8*, 1538.
- [16] Z. Jinghui, L. Shujuan, W. Ruizhi, H. Legan, Z. Milin, *J. Magnesium Alloys* **2018**, *6*, 277.
- [17] Y. Zhang, H. Jiang, Y. Wang, Z. Xu, *Metals* **2020**, *10*, 777.
- [18] K. Huang, K. Marthinsen, Q. Zhao, R. E. Logé, *Prog. Mater. Sci.* **2018**, *92*, 284.
- [19] Z. Zhang, J. Zhang, J. Xie, S. Liu, Y. He, K. Guan, R. Wu, *Scr. Mater.* **2022**, *209*, 114414.
- [20] D. Guan, J. Nutter, J. Sharp, J. Gao, W. Mark Rainforth, *Scr. Mater.* **2017**, *138*, 39.
- [21] L. Gao, R. S. Chen, E. H. Han, *J. Alloys Compd.* **2009**, *481*, 379.
- [22] W. He, E. Zhang, K. Yang, *Mater. Sci. Eng. C* **2010**, *30*, 167.
- [23] L. Xianbin, S. Dayong, S. Yingwei, H. En-hou, *J. Magnesium Alloys* **2017**, *5*, 26.
- [24] S. Jafari, S. E. Harandi, R. K. Singh Raman, *JOM* **2015**, *67*, 1143.
- [25] M. Linderov, A. Brilevsky, D. Merson, A. Danyuk, A. Vinogradov, *Materials* **2022**, *15*, 567.
- [26] B. Q. Shi, R. S. Chen, W. Ke, *Mater. Sci. Eng., A* **2013**, *560*, 62.
- [27] K. Hantzsche, J. Bohlen, J. Wendt, K. U. Kainer, S. B. Yi, D. Letzig, *Scr. Mater.* **2010**, *63*, 725.
- [28] I. Basu, T. Al-Samman, *Acta Mater.* **2014**, *67*, 116.
- [29] J. Meng, L. Sun, Y. Zhang, F. Xue, C. Chu, J. Bai, *Materials* **2020**, *13*, 427.
- [30] D. Xia, Y. Liu, S. Wang, R.-C. Zeng, Y. Liu, Y. Zheng, Y. Zhou, *Sci. China Mater.* **2018**, *62*, 256.
- [31] A. Becerra, M. Pegguleryuz, *J. Mater. Res.* **2008**, *23*, 3379.
- [32] Y. Zeng, B. Jiang, Q. R. Yang, G. F. Quan, J. J. He, Z. T. Jiang, F. S. Pan, *Mater. Sci. Eng. A* **2017**, *700*, 59.
- [33] S.-K. Lee, I.-K. Lee, S.-M. Lee, S.-Y. Lee, *Materials* **2019**, *12*, 3923.
- [34] BS ISO 7802:2013; *Metallic Materials. Wire. Wrapping Test*, British Standards Institute, Geneva, Switzerland **2013**.
- [35] C. D. Barrett, A. Imandoust, H. El Kadiri, *Scr. Mater.* **2018**, *146*, 46.
- [36] J. D. Robson, S. J. Haigh, B. Davis, D. Griffiths, *Metall. Mater. Trans. A* **2016**, *47*, 522.
- [37] M. Nienaber, S. Yi, K. U. Kainer, D. Letzig, J. Bohlen, *Metals* **2020**, *10*, 1208.
- [38] M. T. Pérez-Prado, O. A. Ruano, *Scr. Mater.* **2002**, *46*, 149.